Supplementary Information

Chromatographic NMR spectroscopy: the effect of hollow silica microspheres on magnetic field inhomogeneities and resonance lineshapes

Federico De Biasi,[1] Federico Moro,[2] Diego Frezzato,[1] Federico Rastrelli[1]

[1]Department of Chemical Sciences, Università degli Studi di Padova, Padova, Italy.

[2]Department of Industrial Engineering, Università degli Studi di Padova, Padova, Italy.

Table of Content

1. Generation of the random packings

A double-precision Fortran code has been developed to generate and characterize statistically random packings made of a required number of identical spheres. Let b be the radius of the spheres, and n_0 be the target number of vicinal spheres; two spheres are here considered to be "vicinal" if their centre-to-centre distance is comprised between $2b$ and $3b$. A first sphere is placed in (0,0,0) and an attempt is made to place a number n_0 of vicinal spheres with a uniform spatial distribution. To this purpose, the components of the vector displacement of a candidate vicinal sphere from the central one, are generated by operating in spherical coordinates: by drawing at random three numbers u_1, u_2 and u_3 from the uniform distribution in [0, 1], the spherical coordinates are computed as $\rho = \left[d_{\min}^3 + u_1\left(d_{\max}^3 - d_{\min}^3\right)\right]^{1/3}$ (distance from the reference centre), $\vartheta = \arccos(1 - 2u_2)$ (azimuthal angle) and $\phi = 2\pi\, u_3$ (polar angle). Random numbers are generated by means of the routine "ran2".[1] Then, it is checked if such a candidate sphere does not overlap with all spheres already placed (the list of vicinal spheres is updated to speed up the check). If the candidate sphere is rejected, the drawing is repeated; after 10^6 rejections, the algorithm jumps to the next sphere to be placed. Once the cycle over n_0 attempted placements is completed, the procedure is repeated by treating each of the placed spheres as the new central one. When the required number of spheres is reached, the spheres are ordered according to the increasing distance from the origin. The filling factor is computed as $\mathrm{FF} = n_s(b/R_c)^3$ where $R_c = 10b$ is a chosen cut-off radius and n_s is the number of spheres whose centre fall

at a distance $\leq R_c$ from the origin. With such a kind of growth, each sphere is expected to have about the same statistical properties. The statistical analysis is made *a posteriori*. Two indicators are considered for each sphere: the actual number of vicinal spheres (n_{vic}) and the three eigenvalues of the inertia tensor of the cluster formed by the sphere and the vicinal ones (the division by total mass of the cluster is made to get rid of its variable extension). Average values and standard deviations are computed for each indicator. A homogenous and locally isotropic random packing should feature both a small standard deviation for n_{vic} and closeness of the three eigenvalues within the associated standard deviations. As example, the parameters for the sample with FF $= 0.35$ are the following (obtained by analysing the first 500 spheres from the origin): average n_{vic} equal to 8.4 (with standard deviation of 2.4) and average eigenvalues of the scaled inertia tensor of the clusters equal to 1.63, 1.77 and 1.65 (with standard deviations of the order of 0.65) indicating local isotropy.

2. Calculation of the magnetic field in the presence of hollow spheres

2.1 Dipolar approximation

Calculations at the dipolar approximation level have been implemented by means of two dedicated scripts (notebooks) written in Mathematica 11.1.

The first notebook solves the magnetostatics problem outlined in reference 2 with proper boundary conditions for a single isolated spherical shell (or full sphere) of given permeability immersed in a uniform field $\mathbf{H}_0$. The resulting expression is then mapped onto a collection of spheres whose centres' coordinates can be imported by the user (*e.g.* the Finney pack), and the total **H** field is calculated as the sum of all the contributions from the single spheres. The same notebook can output a figure displaying a 2D section of the magnetic field distribution across the sample (Fig. S1).

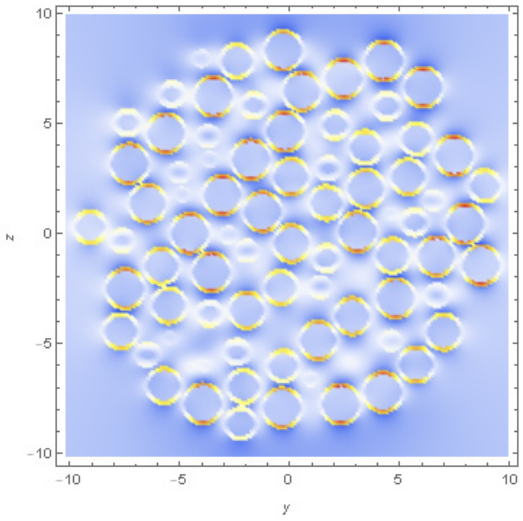

Figure S1. *zy* section ($x = 0$) of the **H** field inside the Finney pack (500 hollow spheres) calculated at the dipolar approximation level.

The second notebook performs a random homogeneous sampling inside a portion of space defined by the user and calculates the field distribution of B_z inside each subdomain (interstices, shells, cavities), providing the associated histograms and probability density functions.

Depending on the number of sampled points, the two notebooks typically evaluate in several minutes when parallelized on four i7-7700 CPU @ 3.60GHz cores. These notebooks are available upon request to the authors.

2.2 Finite Element Method

COMSOL Multiphysics 5.2 has been chosen for the FEM analysis of the magnetostatics problem. The packing structures utilized in the calculations are the Finney pack and the spherical ensembles generated with the algorithm described in section 1. To avoid edge effects in the simulations, a proper number of spheres is considered during the generation of the geometry to build an ensemble with total radius of about 10 times the external radius of a single sphere. The resulting magnetic field is sampled uniformly inside a cube of side $10b$ centered in (0,0,0) (Fig. S2).

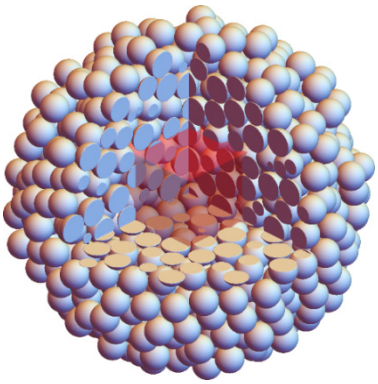

Figure S2. Ensemble of 1000 spheres arranged according to the Finney pack. The field distributions are generated by sampling the magnetic field inside a cube of side $10b$ located at the centre of the ensemble. Note that the emerging volume of the red cube in this picture amounts to 1/8 of the total.

The sampling points are spaced $0.1b$ apart in the three dimensions on a regular cubic grid, for a total of 101^3 sampled points. The absence of edge effects has been verified by further increasing the size of the cluster considered in the FEM analysis and noting that no changes in the magnetic field distributions have occurred.

As an example, the following list summarizes the details of the COMSOL simulation regarding silica 60H shells with $a/b = 0.8$ arranged according to the random packing structure with FF $= 0.35$.

- **Model:** spherical shell agglomerate in a liquid embedded in a spherical air domain (Infinite Element Domain).
- **Formulation:** 3D FEM implementing a reduced scalar potential formulation for magnetostatics; external magnetic field applied in the whole computational domain.
- **Boundary Conditions:** Laplace equation in the magnetic scalar potential solved by using infinite elements to simulate the unbounded air domain.
- **Mesh:** 1,827,150 (2^{nd} order) tetrahedral finite elements.
- **Solution:** the final matrix system of 2^{nd} order FEM is solved in the magnetic scalar potential (2,447,676 degrees of freedom) by a conjugate gradient iterative solver with algebraic multigrid preconditioner.

- **Post-Processing (output data):** longitudinal component of the magnetic field computed in the whole domain on a regular cubic grid.

3. ^{1}H-NMR linewidth in the Redfield limit

In the motional narrowing limit, the transverse relaxation rate $T_{2,\mathrm{DM}}^{-1}$ is expressed by the zero-frequency spectral density (Fourier-Laplace transform) of the time self-correlation function of the magnetic anisotropy (expressed in angular frequency scale) $\Delta\omega(\mathbf{r}) = -\gamma_{\mathrm{H}}(B_z(\mathbf{r}) - \overline{B_z})$, where $B_z(\mathbf{r})$ is the longitudinal component of the magnetic field at the location $\mathbf{r}$, $\overline{B_z}$ is its mean value in the whole volume, and γ_{H} is the gyromagnetic ratio of the proton.[3] Explicitly:

$$T_{2,\mathrm{DM}}^{-1} = \int_0^\infty dt\, G_{\Delta\omega,\Delta\omega}(t) \tag{s.1}$$

$$G_{\Delta\omega,\Delta\omega}(t) = V^{-1} \int d\mathbf{r} \int d\mathbf{r}_0\, \Delta\omega(\mathbf{r}_0)\Delta\omega(\mathbf{r})\, p(\mathbf{r},t|\mathbf{r}_0) \tag{s.2}$$

where $p(\mathbf{r},t|\mathbf{r}_0)$ is the probability to find the spin in $\mathbf{r}$ at time t, given that it was in $\mathbf{r}_0$ at time 0. By combining the above expressions, it follows:

$$T_{2,\mathrm{DM}}^{-1} = V^{-1} \int d\mathbf{r} \int d\mathbf{r}_0\, \Delta\omega(\mathbf{r}_0)\Delta\omega(\mathbf{r}) \int_0^\infty dt\, p(\mathbf{r},t|\mathbf{r}_0) \tag{s.3}$$

For a random walk corresponding to free three-dimensional isotropic and unbounded diffusion with constant diffusion coefficient D, the analytical solution is:

$$p(\mathbf{r},t|\mathbf{r}_0) = (4\pi\, D\, t)^{-\frac{3}{2}}\, \mathrm{e}^{-\frac{|\mathbf{r}-\mathbf{r}_0|^2}{4\,D\,t}} \tag{s.4}$$

where $|\cdot|$ stands for the Euclidean norm. Now consider that:

$$\int_{\tau_\epsilon}^\infty dt\, p(\mathbf{r},t|\mathbf{r}_0) = (4\pi\, D)^{-1}|\mathbf{r}-\mathbf{r}_0|^{-1}\, \mathrm{erf}\left(\frac{|\mathbf{r}-\mathbf{r}_0|}{\sqrt{4D\,\tau_\epsilon}}\right) \tag{s.5}$$

for any $\tau_\epsilon > 0$, where $\mathrm{erf}(\cdot)$ indicates the Error Function. For $|\mathbf{r}-\mathbf{r}_0| \neq 0$, the limit $\tau_\epsilon \to 0^+$ can be taken, yielding:

$$\int_0^\infty dt\, p(\mathbf{r},t|\mathbf{r}_0) = (4\pi\, D)^{-1}|\mathbf{r}-\mathbf{r}_0|^{-1} \tag{s.6}$$

Thus:

$$T_{2,\mathrm{DM}}^{-1} = (4\pi\, D)^{-1} V^{-1} \lim_{L_c \to 0^+} \int d\mathbf{r}_0 \int d\mathbf{r} \frac{\Delta\omega(\mathbf{r}_0)\Delta\omega(\mathbf{r})}{|\mathbf{r}-\mathbf{r}_0|} S_{L_c}(|\mathbf{r}-\mathbf{r}_0|) \tag{s.7}$$

where $S_{L_c}(|\mathbf{r}-\mathbf{r}_0|)$ is a step-function equal to 1 if $|\mathbf{r}-\mathbf{r}_0| \geq L_c$, null otherwise. The contribution at the singularity $\mathbf{r} = \mathbf{r}_0$ is thus removed from the integration. In the practice, the above double-integral has been solved by resorting to the sample-mean stochastic integration strategy.[4] Namely, N_{p} pairs of points $\mathbf{r}_0(i_{\mathrm{p}})$ and $\mathbf{r}(i_{\mathrm{p}})$ with $i_{\mathrm{p}} = 1, \ldots, N_{\mathrm{p}}$ were produced under the requirement $\left|\mathbf{r}(i_{\mathrm{p}}) - \mathbf{r}_0(i_{\mathrm{p}})\right| \neq 0$; each point was randomly drawn from the uniform spatial distribution in the region of volume V. Then, the above double-integral was approximated by:

$$T_{2,\mathrm{DM}}^{-1} = (4\pi D)^{-1} V \frac{1}{N_\mathrm{p}} \sum_{i_\mathrm{p}=1}^{N_\mathrm{p}} \frac{\Delta\omega\left(\mathbf{r}_0(i_\mathrm{p})\right)\Delta\omega\left(\mathbf{r}(i_\mathrm{p})\right)}{\left|\mathbf{r}(i_\mathrm{p}) - \mathbf{r}_0(i_\mathrm{p})\right|} \qquad \text{(s.8)}$$

Clearly, the summation tends to converge as the number of pairs of points increases. The calculations mentioned in the main text were performed by considering 10^8 pairs of points. Each calculation was repeated 10 times to test the robustness of the method.

4. Additional CPMG experiments

Panel **a** of Fig. S3 reports the transverse relaxation rate $1/T_2$ estimated for $CHCl_3$ in $CDCl_3$ via the CPMG pulse sequence (panel **b** of Fig. S3) for different lengths of the semi-echo delay τ in the presence of hollow silica microspheres with $a/b \cong 0.9$. It is evident that there exists a linear relation between ${T_2}^{-1}$ and $\sqrt{\tau}$, at least for small τ values. A τ-dependence of $1/T_2$ is a clear signature of slow motional effects acting on spin relaxation. In addition, it is worth mentioning that the specific $\sqrt{\tau}$ dependence is in accord with the expectation based on the slow-motional theory presented in ref. 5 (developed for a different kind of spin-probe dynamics, but adaptable by analogy to the present case). The physical nature of such slow motional effects can be manifold, like diffusion in field gradients, slow chemical exchange, or slow molecular exchange between environments with different chemical shifts.

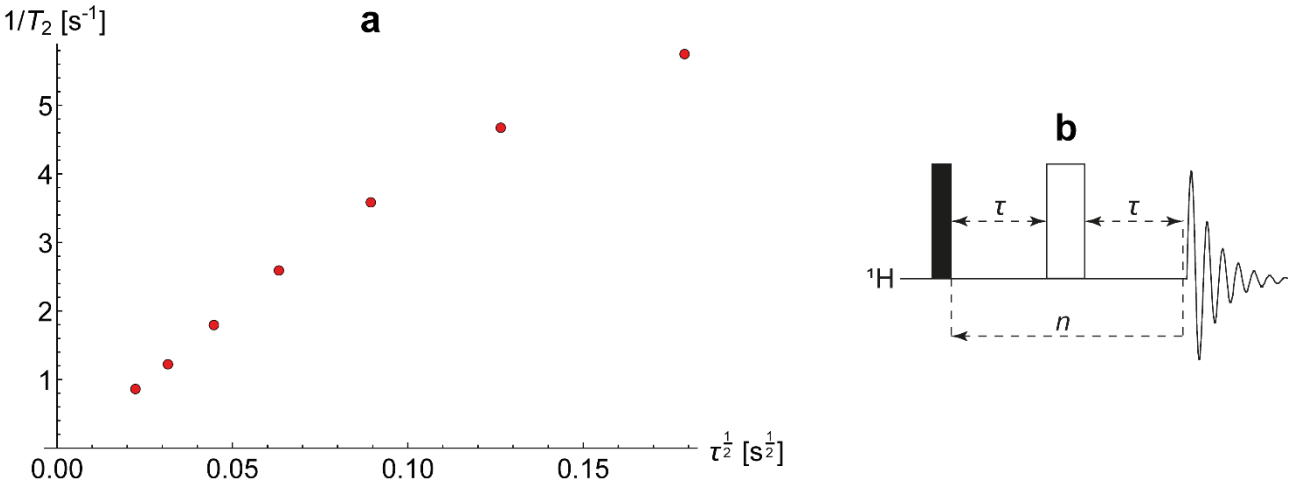

Figure S3. a $1/T_2$ values for $CHCl_3$ in $CDCl_3$ estimated via CPMG experiments for various semi-echo delays τ in the presence of hollow silica microspheres with $a/b \cong 0.9$. **b** CPMG pulse sequence. The full and empty rectangles represent hard 90° and 180° radiofrequency pulses, respectively.

5. ^{1}H-NMR linewidth from single-molecule FIDs

To account for slow motions and the enhanced relaxation within the pores, the ^{1}H-NMR linewidth of the chloroform's signal in the presence of hollow silica microspheres was estimated through the generation of single-molecules Free Induction Decays (FIDs) considering a representative ensemble of spins diffusing in the sample. The FIDs were calculated by sampling the magnetic field in a cube of side $10b$ centered in (0,0,0) (see section 2.2). The magnetic field B_z was sampled every $0.1b$ in each direction, for a total of 101^3 sampled points. 101^3 cubic cells of side $0.1b$ were built around the sampled points, in which the field was assumed to be locally homogeneous and equal to that at the centre of the cell. The combination of all the 101^3 cells

constituted the simulation box of volume V in which the molecules moved, namely a cube centered in (0,0,0) with sides spacing from $-5.05b$ to $5.05b$ (Fig. S4).

The trajectories of the molecules were represented by discretized 3D unrestricted random walks (RWs), generated through the Langevin equation:

$$\mathbf{r}(t + \delta t) = \mathbf{r}(t) + \mathbf{N}\sqrt{2D\,\delta t} \qquad \text{(s.9)}$$

$\mathbf{N} = (u_x, u_y, u_z)$ is a vector containing random variables picked at each new step from the standard normal distribution. The position at time $t + \delta t$ is hence given by the position at time t plus a stochastic contribution that depends on the duration of the imposed timestep δt. A constant (*i.e.*, position-independent) diffusion coefficient was considered, equal to that of $CHCl_3$ in $CDCl_3$ ($D = 1.86 \times 10^{-9}$ m^2 s^{-1}), as the experimental evidence suggested.[6] 10^3 independent random walks were generated in each simulation, to carefully sample the pathways followed by the spins. δt was selected to satisfy the condition $\sqrt{2D\,\delta t} = 20$ nm, namely that the root mean square displacements in the timestep were of the order of $0.03b$. The RWs were computed by initially drawing a random point inside the simulation box with a uniform probability distribution. Periodic boundary conditions were applied to the box, even if they were not formally satisfied by the packing structures. As an example, Fig. S5 shows the box used for the simulations of hollow silica microspheres with $a/b = 0.8$ arranged as in the Finney pack. To check for the presence of spurious boundary effects, some simulations were also repeated using a larger box, sampling the magnetic field inside a cube of side $15b$ (the number of spheres considered in the preliminary FEM analysis was increased as well). No differences in the predicted linewidths were noticed.

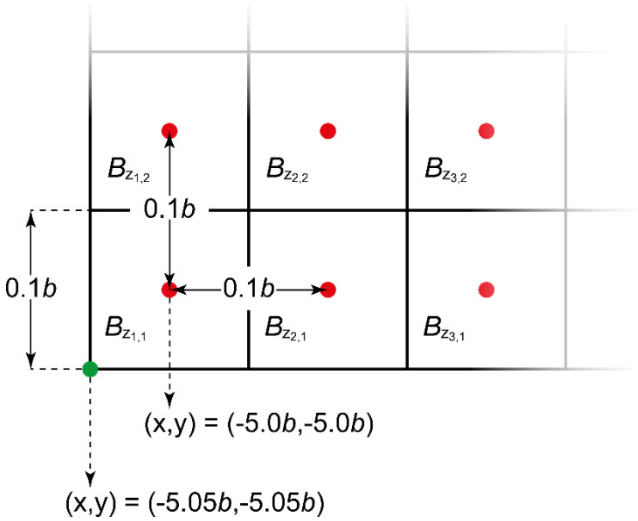

Figure S4. 2D sketch of the simulation box. The red dots portray the sampling points of the magnetic field B_z (from $-5.0b$ to $+5.0b$ in steps of $0.1b$ in the three dimensions). The green dot indicates a vertex of the simulation box, which hence comprises 101^3 cubic cells of side $0.1b$, represented here by the black squares. Consequently, the simulation box consists in a cube centered in (0,0,0) whose sides go from $-5.05b$ to $+5.05b$. The field within a single cell is assumed to be homogeneous.

The single molecules FIDs were built based the RWs data. At each step, the position of the spin (proton of $CHCl_3$) was calculated and its resonance frequency computed according to the B_z value in that position. It was also assumed that the same field was experienced for the entire time step δt. The relevant spin Hamiltonian contained only the Zeeman interaction with the varying component of the local longitudinal magnetic field,[7]

as highlighted in the main text. At each step, it was also verified if the position of the spin fell within a silica shell cell. The criterion by which a cell is defined to be entirely occupied by silica or solvent is based on whether the centre of the cell was comprised or not in a hollow microsphere. Transverse relaxation with a characteristic time $T_{2,\text{pore}}$ was artificially introduced only in the silica-occupied cells to account for both slow motional effects and the enhanced spin relaxation inside the small silica pores.

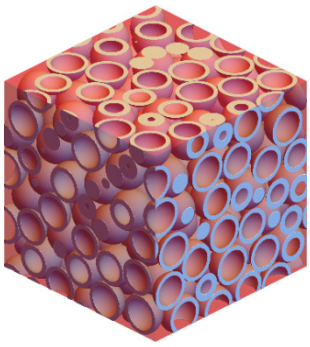

Figure S5. Picture of a simulation box of side $10.1b$ for silica shells with $a/b = 0.8$ arranged as in the Finney pack.

The FID value for a single spin-probe at the n^{th} step of the RW was computed as:

$$\text{FID}_{\text{single spin-probe}}(n) = \cos[-\Delta\omega_{\text{loc}}(n)\,\delta t + \text{phase}] \times \exp\left[-\frac{m(n)\,\delta t}{T_{2,\text{pore}}}\right] \qquad \text{(s.10)}$$

where:

- $\Delta\omega_{\text{loc}}(n)$ is the position-dependent stochastic resonance frequency at the n^{th} step
- the phase is equal to the entire cosine argument at the step $n-1$ (for the initial step, the phase is 0)
- $m(n)$ is a variable that counts how many steps have occurred inside silica-filled cells at the n^{th} step

After the generation of N random walk trajectories, the single FIDs were superimposed to get their ensemble average. The resulting signal was interpolated with a decaying exponential featuring an effective transverse relaxation time T_2^*:

$$\text{FID}(n) = \frac{1}{N}\sum_{i=1}^{N} \text{FID}_{\text{single spin-probe},i}(n) \equiv \exp\left[-\frac{n\,\delta t}{T_2^*}\right] \qquad \text{(s.11)}$$

The linewidth was then computed as $1/(\pi T_2^*)$.

The calculations are performed imposing $N = 10^3$. Each calculation was repeated 6 times to test the robustness of the method. A total FID duration of 0.2 s was simulated (1.86×10^6 steps). The values of the single-molecules FIDs, as well as of the averaged overall FID, were stored only every 10^4 steps. The simulations require MATLAB to run and the code is available on request to the authors.

6. ^{1}H-NMR linewidth calculated for other $T_{2,\text{pore}}$ relaxation times and no $T_{2,\text{pore}}$

The following tables contains the linewidths computed for different values of $T_{2,\text{pore}}$, from 1 ms to 10 ms. The table relative to $T_{2,\text{pore}} = 3$ ms is reported in the main text. All the calculations were performed as mentioned in section 4. The last table (Tab. S10) reports the linewidth values obtained without artificially introducing

any spin relaxation inside the silica cells and it is worth to remind that, in this condition, the linewidths predicted are equal to those calculated by means of Eq. (s.8) (within the statistical uncertainties).

Table S1. $T_{2,pore} = 1$ ms

	$T_{2,pore}$ = 1 ms		FF				
			0.25	**0.30**	**0.35**	**0.40**	**0.62**
60H Silica	***a/b***	**0.5**	73.89 ± 0.06	89.2 ± 0.2	101.5 ± 0.2	107.7 ± 0.2	169.3 ± 0.2
		0.6	64.71 ± 0.04	78.26 ± 0.08	89.1 ± 0.1	94.8 ± 0.2	150.10 ± 0.07
		0.7	52.83 ± 0.04	63.66 ± 0.07	72.62 ± 0.09	77.4 ± 0.1	123.86 ± 0.09
		0.8	37.09 ± 0.04	44.92 ± 0.04	51.39 ± 0.07	54.76 ± 0.05	88.63 ± 0.03
		0.9	17.88 ± 0.01	21.83 ± 0.03	25.00 ± 0.03	26.76 ± 0.02	43.66 ± 0.03
	$T_{2,pore}$ = 1 ms		FF				
			0.25	**0.30**	**0.35**	**0.40**	**0.62**
RP Silica	***a/b***	**0.5**	67.49 ± 0.09	83.2 ± 0.1	94.4 ± 0.2	102.1 ± 0.1	166.40 ± 0.07
		0.6	60.1 ± 0.1	73.9 ± 0.2	83.9 ± 0.2	90.6 ± 0.1	148.0 ± 0.1
		0.7	49.42 ± 0.05	60.86 ± 0.09	69.36 ± 0.07	74.7 ± 0.1	122.11 ± 0.06
		0.8	35.61 ± 0.02	43.64 ± 0.04	49.77 ± 0.04	53.61 ± 0.05	87.64 ± 0.07
		0.9	17.56 ± 0.02	21.55 ± 0.01	24.62 ± 0.04	26.43 ± 0.02	43.32 ± 0.02

Table S2. $T_{2,pore} = 2$ ms

	$T_{2,pore}$ = 2 ms		FF				
			0.25	**0.30**	**0.35**	**0.40**	**0.62**
60H Silica	***a/b***	**0.5**	41.27 ± 0.08	48.17 ± 0.09	55.0 ± 0.1	57.4 ± 0.1	86.51 ± 0.06
		0.6	35.57 ± 0.05	41.84 ± 0.08	47.74 ± 0.08	49.95 ± 0.06	76.55 ± 0.02
		0.7	28.15 ± 0.06	33.50 ± 0.05	38.35 ± 0.07	40.24 ± 0.05	62.94 ± 0.04
		0.8	19.39 ± 0.04	23.36 ± 0.03	26.66 ± 0.03	28.24 ± 0.05	44.96 ± 0.02
		0.9	9.17 ± 0.01	11.126 ± 0.009	12.73 ± 0.01	13.57 ± 0.01	22.035 ± 0.007
	$T_{2,pore}$ = 2 ms		FF				
			0.25	**0.30**	**0.35**	**0.40**	**0.62**
RP Silica	***a/b***	**0.5**	34.61 ± 0.04	42.23 ± 0.08	48.18 ± 0.04	51.72 ± 0.07	83.65 ± 0.03
		0.6	30.65 ± 0.03	37.43 ± 0.04	42.64 ± 0.04	45.83 ± 0.02	74.25 ± 0.04
		0.7	25.13 ± 0.03	30.82 ± 0.03	35.06 ± 0.04	37.68 ± 0.03	61.21 ± 0.02
		0.8	17.94 ± 0.03	21.97 ± 0.02	25.06 ± 0.03	26.91 ± 0.02	43.94 ± 0.02
		0.9	8.810 ± 0.006	10.816 ± 0.002	12.372 ± 0.006	13.261 ± 0.007	21.719 ± 0.009

Table S3. $T_{2,pore} = 4$ ms

	$T_{2,pore}$ = 4 ms		FF				
			0.25	**0.30**	**0.35**	**0.40**	**0.62**
60H Silica	***a/b***	**0.5**	24.4 ± 0.2	27.8 ± 0.1	31.5 ± 0.1	31.90 ± 0.08	45.01 ± 0.04
		0.6	20.5 ± 0.2	23.58 ± 0.04	26.84 ± 0.09	27.41 ± 0.09	39.71 ± 0.04
		0.7	15.96 ± 0.05	18.33 ± 0.06	21.06 ± 0.07	21.64 ± 0.06	32.49 ± 0.04
		0.8	10.55 ± 0.02	12.47 ± 0.02	14.26 ± 0.01	14.82 ± 0.02	23.05 ± 0.02
		0.9	4.788 ± 0.008	5.748 ± 0.005	6.584 ± 0.007	6.963 ± 0.007	11.196 ± 0.008
	$T_{2,pore}$ = 4 ms		FF				
			0.25	**0.30**	**0.35**	**0.40**	**0.62**
RP Silica	***a/b***	**0.5**	17.86 ± 0.04	21.65 ± 0.02	24.66 ± 0.04	26.39 ± 0.03	42.06 ± 0.02
		0.6	15.75 ± 0.01	19.12 ± 0.03	21.70 ± 0.02	23.27 ± 0.03	37.36 ± 0.02
		0.7	12.84 ± 0.02	15.656 ± 0.009	17.79 ± 0.04	19.07 ± 0.03	30.77 ± 0.01
		0.8	9.129 ± 0.008	11.103 ± 0.009	12.678 ± 0.008	13.584 ± 0.009	22.059 ± 0.006
		0.9	4.436 ± 0.02	5.436 ± 0.002	6.214 ± 0.004	6.651 ± 0.006	10.883 ± 0.002

Table S4. $T_{2,pore} = 5$ ms

	$T_{2,pore} =$ 5 ms		FF				
			0.25	**0.30**	**0.35**	**0.40**	**0.62**
60H Silica	a/b	**0.5**	21.0 ± 0.1	23.2 ± 0.1	26.7 ± 0.1	26.9 ± 0.1	36.68 ± 0.04
		0.6	17.6 ± 0.1	19.88 ± 0.05	22.6 ± 0.1	22.85 ± 0.08	32.33 ± 0.07
		0.7	13.38 ± 0.03	15.31 ± 0.04	17.58 ± 0.07	17.90 ± 0.05	26.40 ± 0.04
		0.8	8.86 ± 0.02	10.26 ± 0.03	11.76 ± 0.02	12.12 ± 0.03	18.69 ± 0.03
		0.9	3.896 ± 0.005	4.668 ± 0.008	5.353 ± 0.008	5.637 ± 0.006	9.036 ± 0.005
	$T_{2,pore} =$ 5 ms		FF				
			0.25	**0.30**	**0.35**	**0.40**	**0.62**
RP Silica	a/b	**0.5**	14.54 ± 0.02	17.56 ± 0.02	20.00 ± 0.03	21.33 ± 0.02	33.77 ± 0.02
		0.6	12.78 ± 0.02	15.45 ± 0.01	17.59 ± 0.02	18.753 ± 0.006	29.95 ± 0.01
		0.7	10.38 ± 0.02	12.620 ± 0.008	14.372 ± 0.004	15.33 ± 0.02	24.677 ± 0.006
		0.8	7.33 ± 0.01	8.921 ± 0.007	10.201 ± 0.004	10.909 ± 0.004	17.675 ± 0.005
		0.9	3.563 ± 0.001	4.359 ± 0.001	4.984 ± 0.002	5.337 ± 0.001	8.720 ± 0.002

Table S5. $T_{2,pore} = 6$ ms

	$T_{2,pore} =$ 6 ms		FF				
			0.25	**0.30**	**0.35**	**0.40**	**0.62**
60H Silica	a/b	**0.5**	18.8 ± 0.2	20.82 ± 0.09	23.6 ± 0.2	23.6 ± 0.1	31.12 ± 0.02
		0.6	15.6 ± 0.1	17.37 ± 0.06	19.95 ± 0.06	19.89 ± 0.08	27.38 ± 0.04
		0.7	11.82 ± 0.07	13.34 ± 0.05	15.17 ± 0.01	15.40 ± 0.04	22.30 ± 0.04
		0.8	7.70 ± 0.02	8.82 ± 0.02	10.11 ± 0.02	10.39 ± 0.03	15.81 ± 0.02
		0.9	3.31 ± 0.01	3.952 ± 0.006	4.541 ± 0.006	4.726 ± 0.003	7.597 ± 0.004
	$T_{2,pore} =$ 6 ms		FF				
			0.25	**0.30**	**0.35**	**0.40**	**0.62**
RP Silica	a/b	**0.5**	12.29 ± 0.02	14.75 ± 0.02	16.82 ± 0.02	17.89 ± 0.03	28.231 ± 0.007
		0.6	10.77 ± 0.01	12.99 ± 0.02	14.78 ± 0.02	15.77 ± 0.01	25.018 ± 0.008
		0.7	8.747 ± 0.009	10.58 ± 0.01	12.05 ± 0.01	12.865 ± 0.007	20.608 ± 0.006
		0.8	6.161 ± 0.004	7.484 ± 0.004	8.531 ± 0.006	9.120 ± 0.004	14.757 ± 0.003
		0.9	2.981 ± 0.001	3.640 ± 0.001	4.165 ± 0.001	4.456 ± 0.001	7.274 ± 0.002

Table S6. $T_{2,pore} = 7$ ms

	$T_{2,pore} =$ 7 ms		FF				
			0.25	**0.30**	**0.35**	**0.40**	**0.62**
60H Silica	a/b	**0.5**	17.41 ± 0.07	18.84 ± 0.06	21.46 ± 0.07	21.19 ± 0.09	27.16 ± 0.03
		0.6	14.31 ± 0.06	15.60 ± 0.07	17.7 ± 0.1	17.70 ± 0.08	23.80 ± 0.08
		0.7	10.60 ± 0.03	11.83 ± 0.05	13.67 ± 0.07	13.63 ± 0.02	19.49 ± 0.03
		0.8	6.79 ± 0.01	7.76 ± 0.02	8.92 ± 0.03	9.10 ± 0.03	13.71 ± 0.01
		0.9	2.917 ± 0.007	3.444 ± 0.005	3.963 ± 0.007	4.126 ± 0.003	6.554 ± 0.007
	$T_{2,pore} =$ 7 ms		FF				
			0.25	**0.30**	**0.35**	**0.40**	**0.62**
RP Silica	a/b	**0.5**	10.649 ± 0.006	12.817 ± 0.003	14.56 ± 0.02	15.46 ± 0.01	24.265 ± 0.008
		0.6	9.36 ± 0.02	11.272 ± 0.007	12.795 ± 0.006	13.610 ± 0.007	21.510 ± 0.007
		0.7	7.574 ± 0.004	9.128 ± 0.006	10.41 ± 0.01	11.06 ± 0.02	17.708 ± 0.008
		0.8	5.313 ± 0.002	6.441 ± 0.006	7.360 ± 0.007	7.853 ± 0.002	12.675 ± 0.002
		0.9	2.562 ± 0.001	3.127 ± 0.002	3.576 ± 0.002	3.827 ± 0.001	6.242 ± 0.002

Table S7. $T_{2,pore} = 8$ ms

	$T_{2,pore} =$ 8 ms		FF				
			0.25	**0.30**	**0.35**	**0.40**	**0.62**
60H Silica	a/b	**0.5**	16.0 ± 0.1	17.1 ± 0.1	19.6 ± 0.1	19.15 ± 0.08	24.26 ± 0.02
		0.6	13.2 ± 0.1	14.36 ± 0.04	16.2 ± 0.01	16.12 ± 0.05	21.15 ± 0.06
		0.7	9.86 ± 0.06	10.75 ± 0.04	12.44 ± 0.07	12.25 ± 0.03	17.27 ± 0.02
		0.8	6.15 ± 0.02	7.02 ± 0.03	8.06 ± 0.03	8.151 ± 0.009	12.14 ± 0.02
		0.9	2.584 ± 0.005	3.050 ± 0.006	3.518 ± 0.007	3.654 ± 0.007	5.787 ± 0.002
	$T_{2,pore} =$ 8 ms		FF				
			0.25	**0.30**	**0.35**	**0.40**	**0.62**
RP Silica	a/b	**0.5**	9.47 ± 0.02	11.32 ± 0.01	12.91 ± 0.01	13.66 ± 0.01	21.289 ± 0.007
		0.6	8.28 ± 0.02	9.91 ± 0.02	11.264 ± 0.009	11.97 ± 0.02	18.862 ± 0.008
		0.7	6.69 ± 0.01	8.050 ± 0.009	9.17 ± 0.01	9.764 ± 0.005	15.526 ± 0.004
		0.8	4.681 ± 0.003	5.664 ± 0.002	6.468 ± 0.005	6.890 ± 0.004	11.114 ± 0.004
		0.9	2.245 ± 0.002	2.746 ± 0.001	3.138 ± 0.001	3.354 ± 0.001	5.467 ± 0.001

Table S8. $T_{2,pore} = 9$ ms

	$T_{2,pore} =$ 9 ms		FF				
			0.25	**0.30**	**0.35**	**0.40**	**0.62**
60H Silica	a/b	**0.5**	15.0 ± 0.2	15.9 ± 0.1	18.3 ± 0.1	18.00 ± 0.07	21.97 ± 0.04
		0.6	12.2 ± 0.1	13.4 ± 0.1	15.0 ± 0.1	14.8 ± 0.1	19.18 ± 0.05
		0.7	9.20 ± 0.05	9.99 ± 0.05	11.37 ± 0.09	11.31 ± 0.05	15.56 ± 0.03
		0.8	5.65 ± 0.02	6.39 ± 0.02	7.40 ± 0.03	7.423 ± 0.009	10.90 ± 0.02
		0.9	2.35 ± 0.01	2.753 ± 0.006	3.175 ± 0.005	3.296 ± 0.004	5.183 ± 0.006
	$T_{2,pore} =$ 9 ms		FF				
			0.25	**0.30**	**0.35**	**0.40**	**0.62**
RP Silica	a/b	**0.5**	8.54 ± 0.03	10.15 ± 0.01	11.62 ± 0.02	12.25 ± 0.02	18.97 ± 0.01
		0.6	7.43 ± 0.01	8.89 ± 0.01	10.15 ± 0.01	10.733 ± 0.008	16.803 ± 0.007
		0.7	5.98 ± 0.01	7.20 ± 0.01	8.20 ± 0.01	8.711 ± 0.005	13.822 ± 0.003
		0.8	4.191 ± 0.003	5.052 ± 0.004	5.773 ± 0.004	6.147 ± 0.004	9.899 ± 0.004
		0.9	2.002 ± 0.002	2.444 ± 0.001	2.795 ± 0.002	2.985 ± 0.001	4.866 ± 0.001

Table S9. $T_{2,pore} = 10$ ms

	$T_{2,pore} =$ 10 ms		FF				
			0.25	**0.30**	**0.35**	**0.40**	**0.62**
60H Silica	a/b	**0.5**	14.23 ± 0.07	15.3 ± 0.2	17.3 ± 0.1	16.8 ± 0.2	20.14 ± 0.05
		0.6	11.52 ± 0.05	12.47 ± 0.06	14.37 ± 0.05	13.80 ± 0.06	17.49 ± 0.06
		0.7	8.50 ± 0.08	9.22 ± 0.06	10.70 ± 0.08	10.49 ± 0.07	14.14 ± 0.02
		0.8	5.29 ± 0.03	5.92 ± 0.03	6.86 ± 0.04	6.82 ± 0.03	9.93 ± 0.02
		0.9	2.14 ± 0.01	2.510 ± 0.008	2.912 ± 0.004	2.993 ± 0.003	4.715 ± 0.006
	$T_{2,pore} =$ 10 ms		FF				
			0.25	**0.30**	**0.35**	**0.40**	**0.62**
RP Silica	a/b	**0.5**	7.82 ± 0.02	9.21 ± 0.02	10.52 ± 0.01	11.081 ± 0.007	17.13 ± 0.01
		0.6	6.78 ± 0.01	8.09 ± 0.02	9.19 ± 0.01	9.73 ± 0.01	15.154 ± 0.003
		0.7	5.431 ± 0.009	6.525 ± 0.006	7.444 ± 0.005	7.882 ± 0.008	12.470 ± 0.004
		0.8	3.782 ± 0.006	4.574 ± 0.003	5.228 ± 0.005	5.559 ± 0.004	8.918 ± 0.001
		0.9	1.809 ± 0.001	2.204 ± 0.002	2.526 ± 0.002	2.693 ± 0.001	4.385 ± 0.001

Table S10. Without $T_{2,pore}$

60H Silica	**NO $T_{2,pore}$**		**FF**				
			0.25	**0.30**	**0.35**	**0.40**	**0.62**
	a*/*b	**0.5**	7.3 ± 0.2	6.5 ± 0.3	7.6 ± 0.3	6.2 ± 0.2	3.41 ± 0.08
		0.6	5.5 ± 0.3	4.9 ± 0.3	5.7 ± 0.3	4.7 ± 0.2	2.67 ± 0.08
		0.7	3.5 ± 0.2	3.2 ± 0.2	3.6 ± 0.2	2.93 ± 0.08	1.95 ± 0.09
		0.8	1.71 ± 0.05	1.6 ± 0.1	1.81 ± 0.04	1.49 ± 0.02	1.17 ± 0.07
		0.9	0.39 ± 0.01	0.37 ± 0.02	0.43 ± 0.02	0.35 ± 0.02	0.37 ± 0.03
RP Silica	**NO $T_{2,pore}$**		**FF**				
			0.25	**0.30**	**0.35**	**0.40**	**0.62**
	a*/*b	**0.5**	1.08 ± 0.02	0.98 ± 0.01	1.04 ± 0.03	0.97 ± 0.02	0.45 ± 0.01
		0.6	0.76 ± 0.01	0.67 ± 0.03	0.78 ± 0.04	0.64 ± 0.02	0.37 ± 0.01
		0.7	0.480 ± 0.008	0.43 ± 0.01	0.49 ± 0.02	0.41 ± 0.02	0.269 ± 0.009
		0.8	0.231 ± 0.004	0.212 ± 0.005	0.24 ± 0.01	0.20 ± 0.01	0.161 ± 0.005
		0.9	0.054 ± 0.002	0.050 ± 0.001	0.056 ± 0.003	0.047 ± 0.002	0.052 ± 0.002

7. Magnetic field gradient distributions

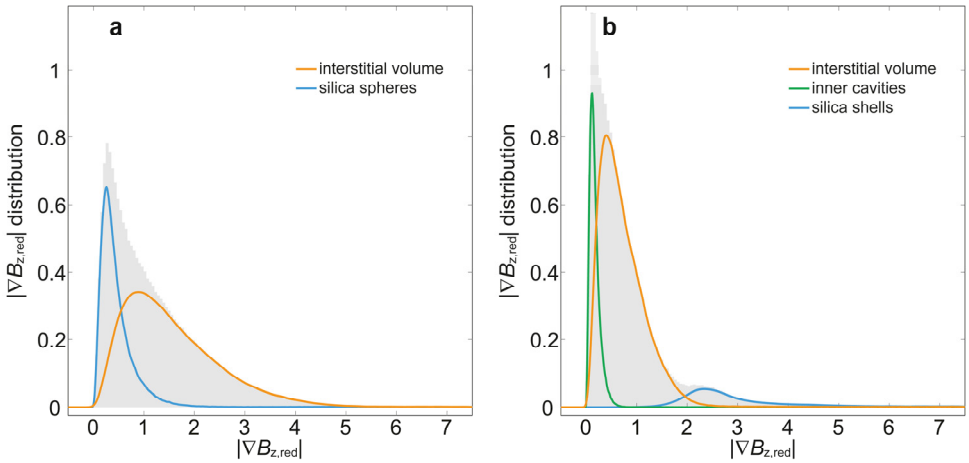

Figure S6. Reduced magnetic field gradient distributions[8] for silica spheres with unitary external radius *b* arranged according to the lattice with FF = 0.35. **a** full spheres. **b** hollow spheres with $a/b = 0.8$.

References

1 W. H. Press, S. A. Teukolsky, W. T. Vetterling and B. P. Flannery, *Numerical Recipes in Fortran 77: The art of scientific computing Vol. 1*, Cambdridge University Press, Second Edit., 1997.

2 J. D. Jackson, *Classical Electrodynamics*, John Wiley & Sons, Ltd, Third Edit., 1999.

3 A. G. Redfield, *The Theory of Relaxation Processes*, 1965, pp 1–32.

4 M. P. Allen and D. J. Tildesley, *Computer simulation of liquids*, Oxford University Press, First Edit., 1993.

5 D. Frezzato, G. Kothe and G. J. Moro, *J. Phys. Chem. B*, 2001, **105**, 1281–1292.

6 R. E. Hoffman, H. Arzuan, C. Pemberton, A. Aserin and N. Garti, *J. Magn. Reson.*, 2008, **194**, 295–299.

7 J. Kowalewski and L. Mäler, *Nuclear Spin Relaxation in Liquids: Theory, Experiments and Applications*, Taylor & Francis Group, First Edit., 2006.

8 B. Audoly, P. N. Sen, S. Ryu and Y.-Q. Song, *J. Magn. Reson.*, 2003, **164**, 154–159.